[DOI]10.12016/j.issn.2096-1456.202660077

·基础研究·

双网络水凝胶-微针抑制口腔鳞状细胞癌复发及促进组织修复的研究

储梦娴，　叶修文，　谢稀，　廖金凤
口腔疾病防治全国重点实验室 国家口腔医学中心 口腔疾病国家临床医学研究中心 四川大学华西口腔医院，四川 成都（610041）

【摘要】　目的　探讨双网络水凝胶-微针在抑制口腔鳞状细胞癌（OSCC）复发及组织修复中的治疗效果，为OSCC的临床治疗提供依据。**方法**　通过壳聚糖（CS）与聚乙二醇-二苯甲醛（PEG-CHO）形成的席夫碱凝胶，以及海藻酸钠（SA）与Cu^{2+}的配位交联水凝胶，共同构建CS/PEG-CHO/SA/Cu^{2+}（CPSC）双网络水凝胶基底，并经扫描电镜（SEM）、傅里叶变换红外光谱（FTIR）、流变及溶胀实验表征并优化水凝胶配比。随后，将5-氟尿嘧啶（5-FU）和金纳米棒（GNR）引入CPSC水凝胶中，制备5-FU/GNR（FG）微针（MN）。测定FG微针的力学及溶解性能，通过近红外光（NIR）照射和热成像评估其光热性能。将FG微针与小鼠成纤维细胞系L929细胞和人口腔黏膜上皮细胞系GMSM-K细胞共培养2 d和4 d，细胞计数试剂盒-8法（CCK-8）和死/活细胞染色观察细胞存活情况。将人OSCC细胞系Cal-27细胞分为Control组（完全培养基组），5-FU MN组（负载5-FU微针共培养组），GNR MN+NIR组（负载GNR微针共培养并接受0.4 W/cm^2的NIR照射5 min组）和FG MN+NIR组（负载5-FU和GNR微针共培养并接受相同NIR照射组），共培养24 h和48 h，CCK-8法和死/活细胞染色观察细胞存活情况。动物实验经实验动物伦理委员会批准，建立Cal-27源性皮下OSCC术后复发BALB/c-nu裸鼠模型，分为Control组、5-FU MN组、GNR MN+NIR组和FG MN+NIR组，Control组不做处理，其余组分别敷贴对应微针，GNR MN+NIR组和FG MN+NIR组进行NIR照射（0.4 W/cm^2，5 min）。7 d后切除肿瘤测量体积，14 d观察肿瘤复发及创面愈合情况。**结果**　成功构建具有良好的力学和溶解性能的双网络水凝胶-微针，其在近红外光照射5 min后升温至48.4 ℃，达到有效杀伤肿瘤的温度。CCK-8和死/活细胞染色观察结果显示，FG微针对L929和GMSM-K细胞活力无影响，细胞相容性良好，FG MN+NIR组的Cal-27细胞活力低于其余3组，差异具有统计学意义（$P < 0.000\ 1$）。在裸鼠皮下接种Cal-27细胞，7 d后切除的肿瘤，各组肿瘤体积差异无统计学意义，造模成功。术后14 d Control组肿瘤完全复发且创面未愈合，5-FU MN组和GNR MN+NIR组轻度复发，创面部分愈合，FG MN+NIR组在抑制肿瘤复发和促进组织修复方面均优于其余各组，差异具有统计学意义（$P < 0.000\ 1$）。**结论**　双网络水凝胶-微针通过化疗-光热联合治疗，可有效抑制BALB/c-nu裸鼠Cal-27源性皮下OSCC术后肿瘤复发并促进组织修复。

【关键词】　双网络水凝胶；　5-氟尿嘧啶；　金纳米棒；　微针；　光热治疗；　口腔鳞状细胞癌；　肿瘤复发；　组织修复
【中图分类号】　R78　**【文献标志码】**　A　**【文章编号】**　2096-1456（2026）08-0757-14
【引用著录格式】　储梦娴，叶修文，谢稀，等. 双网络水凝胶-微针抑制口腔鳞状细胞癌复发及促进组织修复的研究[J]. 口腔疾病防治, 2026, 34(8): 757-770. doi:10.12016/j.issn.2096-1456.202660077.

微信公众号

Study on inhibition of oral squamous cell carcinoma recurrence and promotion of tissue repair *via* a dual-network hydrogel-microneedle

CHU Mengxian, YE Xiuwen, XIE Xi, LIAO Jinfeng.　State Key Laboratory of Oral Diseases & National Center for Stomatology & National Clinical Research Center for Oral Diseases & West China Hospital of Stomatology, Sichuan University, Chengdu 610041, Sichuan, China

【收稿日期】2026-02-25；　**【修回日期】**2026-05-07
【基金项目】国家自然科学基金项目（32171354）
【作者简介】储梦娴，硕士研究生在读，Email：2418576121@qq.com
【通信作者】廖金凤，教授，博士，Email：liaojinfeng.762@163.com

Corresponding author: LIAO Jinfeng, Email: liaojinfeng.762@163.com

【Abstract】 Objective To investigate the therapeutic effect of a dual-network hydrogel-microneedle (MN) on inhibiting oral squamous cell carcinoma (OSCC) recurrence and promoting tissue repair, thereby providing a foundation for the clinical treatment of OSCC. **Methods** A Schiff base hydrogelformed between chitosan (CS) and poly(ethylene glycol) dibenzaldehyde (PEG-CHO), combined witha coordination-crosslinked hydrogel formed between sodium alginate (SA) and Cu^{2+}, were jointly integrated to form the CS/PEG-CHO/SA/Cu^{2+} (CPSC) dual-network hydrogel base. The hydrogel formulation was optimized based on characterization by scanning electron microscopy, Fourier transform infrared spectroscopy, rheology, and swelling tests. Subsequently, 5-fluorouracil (5-FU) and gold nanorod (GNR) were incorporated into the CPSC hydrogel to fabricate an MN loaded with 5-FU/GNR (FG). The mechanical strength and dissolution behavior of FG MNs were characterized, and their photothermal performance was evaluated under near-infrared (NIR) irradiation using thermal imaging. The mouse fibroblast cell line L929 cells and the human oral mucosal epithelial-derived cell line GMSM-K cells were co-cultured with FG MNs for 2 and 4 days, respectively, and cell viability was assessed by the Cell Counting Kit-8 (CCK-8) assay and dead/live staining. Separately, the human tongue OSCC cell line Cal-27 cells were divided into four groups: a control group (cultured in complete medium), 5-FU MN group (co-cultured with 5-FU-loaded MNs), GNR MN + NIR group (co-cultured with GNR-loaded MNs followed by NIR irradiation at 0.4 W/cm^2 for 5 min), and FG MN + NIR group (co-cultured with FG MNs followed by identical NIR irradiation). After 24 and 48 h of co-culture, Cal-27 cell viability was assessed using both CCK-8 assay and dead/live staining. All animal experiments were approved by the Institutional Animal Ethics Committee. A subcutaneous Cal-27-derived OSCC postoperative recurrence model was established in BALB/c nude mice. The mice were divided into four groups: a control group, 5-FU MN group, GNR MN + NIR group, and FG MN + NIR group. Mice in the control group received no intervention, while the other groups were treated with the corresponding MN patches. Additionally, the GNR MN + NIR and FG MN + NIR groups received NIR irradiation (0.4 W/cm^2, 5 min). Tumors were excised and their volumes measured on day 7, and tumor recurrence and wound healing were assessed on day 14. **Results** A dual-network hydrogel-MN was successfully constructed, demonstrating favorable mechanical and dissolution properties. Upon NIR irradiation for 5 min, the temperature rapidly increased to 48.4°C, reaching the threshold for effective tumor ablation. CCK-8 and dead/live staining results showed that FG MNs exhibited no cytotoxicity toward L929 and GMSM-K cells, indicating good cytocompatibility. However, Cal-27 cell viability in the chemotherapy-photothermal combination group was lower than that in the other three groups, with a statistical difference ($P < 0.0001$). In the nude mouse model, subcutaneous Cal-27 tumors were resected 7 days post-implantation. No statistical difference in tumor volume was observed among groups at this timepoint, confirming successful model establishment. By postoperative day 14, the control group displayed complete tumor recurrence with unhealed wounds, while the 5-FU and GNR MN + NIR groups showed mild recurrence and partial wound healing. The FG MN + NIR group demonstrated superior efficacy in both inhibiting tumor recurrence and promoting tissue repair compared with all other groups, with a statistical difference ($P < 0.0001$). **Conclusion** The dual-network hydrogel-MN system effectively suppresses postoperative recurrence of Cal-27-derived subcutaneous OSCC and promotes tissue repair through chemo-photothermal combined therapy.

【Key words】 dual-network hydrogel; 5-fluorouracil; gold nanorods; microneedles; photothermal therapy; oral squamous cell carcinoma; neoplasm recurrence; tissue repair

J Prev Treat Stomatol Dis, 2026, 34(8): 757-770.

口腔癌是全球常见的恶性肿瘤，其中口腔鳞状细胞癌（oral squamous cell carcinoma，OSCC）约占90%[1]。尽管手术、放疗和化疗等传统手段取得了一定进展，但临床仍面临诸多挑战：手术难以彻底清除浸润性癌细胞，术后复发率高达50%~60%[2]。全身化疗药物如5-氟尿嘧啶（5-fluorouracil，5-FU）虽能抑制肿瘤增殖[3]，但其非特异性分布易引发骨髓抑制[4]、胃肠道反应[5]等全身毒性，且肿瘤微环境的异质性和耐药性进一步限制了疗效[6]。而且，OSCC术后常因复杂的口腔环境而延缓创面修复，延迟愈合的创面会通过释放白细胞介素-6（interleukin-6，IL-6）和肿瘤坏死因子-α（tumor necrosis factor-alpha，TNF-α）等促炎因子[7]和基质金属蛋白酶破坏细胞外基质稳态[8]，形成利于残留肿瘤细胞

增殖的微环境[9]。创伤修复障碍与持续炎症相互作用下,OSCC术后复发风险进一步升高。因此亟需构建一种可局部应用的治疗材料,通过精准递送药物降低全身毒性,同时协同抑制OSCC复发并促进创面修复。

本研究构建了一种基于双网络水凝胶的微针(microneedle,MN)递送体系,用于OSCC术后的局部联合治疗。利用微针的微创穿透、高效载药及局部作用特性[10-11],通过在微针中负载5-FU与金纳米棒(gold nanorod,GNR),并采用壳聚糖(chitosan,CS)与聚乙二醇-二苯甲醛(polyethylene glycol dibenzaldehyde,PEG-CHO)形成的席夫碱水凝胶,以及海藻酸钠(sodium alginate,SA)与Cu^{2+}配位交联水凝胶共同构建的CS/PEG-CHO/SA/Cu^{2+}(chitosan/polyethylene glycol dibenzaldehyde/sodium alginate/Cu^{2+},CPSC)双网络水凝胶作为基底。该设计旨在通过微针实现角质层穿透,在肿瘤残留区域精准释放药物,结合光热与化疗协同作用,并利用水凝胶的生物相容性同步启动组织修复。

5-FU广泛用于实体瘤化疗,而通过微针介导的局部递送可有效缓解其全身给药带来的毒性[12]。GNR在近红外光(near-infrared,NIR)照射下可产生局部高温,直接杀伤肿瘤细胞。同时,光热效应可增强肿瘤细胞膜通透性,促进5-FU胞内摄取,实现化疗-光热协同治疗[13]。微针的基底CPSC双网络水凝胶兼具生物相容性与促修复功能,其三维多孔结构提供促进细胞黏附和增殖的微环境,加速创面愈合,减少感染与瘢痕形成[14-15]。本研究通过体外细胞实验和体内动物实验探讨负载5-FU与GNR的CPSC双网络水凝胶-微针在抑制OSCC复发及促进组织修复中的治疗效果,以期为OSCC的临床治疗提供新的实验依据。

1　材料和方法

1.1　主要材料与仪器

1.1.1　材料　人舌OSCC细胞系Cal-27、小鼠结缔组织成纤维细胞系L929和人口腔黏膜上皮细胞系GMSM-K由四川大学口腔疾病防治国家重点实验室实验室提供。所有BALB/c-nu裸鼠由成都达硕动物实验有限公司提供(实验动物生产许可证号:SCXK(川)2020-030)。

透明质酸钠(H874944,麦克林,中国),壳聚糖(C434547,阿拉丁,中国),聚乙二醇-二苯甲醛(C850235,麦克林,中国),海藻酸钠(SA)(S100126,阿拉丁,中国),五水合硫酸铜(C836340,麦克林,中国),5-FU(MB1273,美仑生物,中国),金纳米棒(GNR)(G486026,阿拉丁,中国),无水乙醇(E809059,麦克林,中国),DMEM培养基(C11995500BT,Gbico,美国)、胎牛血清(AUS-01S-02,Cell-Box,美国)、PBS缓冲液(C10010500BT,Gbico,美国)、胰蛋白酶(2520056,Gbico,美国),T25细胞培养皿(721013,NEST,中国),细胞孔板(703011,NEST,中国),细胞计数试剂盒-8(cell counting kit-8,CCK-8,No. K1018,APE×BIO,美国),死/活细胞染色试剂盒(CA1630,索莱宝,中国),4%多聚甲醛通用型组织固定液(BL539A,Biosharp,中国),异氟烷(R510-22-10,瑞沃德,中国)。

1.1.2　仪器　扫描电镜(scanning electron microscopy,SEM)(JSM-5900LV,JEOL,日本),细胞培养箱(Forma Steri-Cult,Thermo Scientific,美国),流变仪(379-0340,Thermo Scientific,美国),常温离心机(LEGENDMICRO17R,Thermo Scientific,美国),傅里叶红外光谱仪(INVENIO,Bruker,美国),酶标仪(Varioskan LUX,Thermo Fisher,美国),纯水仪(C8673,Millipore,美国),体式显微镜(SZX16,Olympus,日本),荧光倒置显微镜(DMI8,Leica,德国),移液器(Research plus,Eppendorf,德国),热成像仪(FOTRIC 220S,飞础科,中国),近红外激发器(MW-RIR-808/1~50mW,镭仕,中国),冷冻干燥箱(Cryodry CD8,博劢行,中国),高速冷冻离心机(HC-4516R,中科中佳,中国),真空干燥箱(DZF-1,永光明,中国)。

1.2　双网络水凝胶的制备及表征

将45 mL壳聚糖(CS)(6%,w/v)溶液与20 mL的聚乙二醇-二苯甲醛(PEG-CHO)(30%,w/v)溶液搅拌混合均匀,制备成席夫碱水凝胶,记为CP。将海藻酸钠(SA)溶液(2.0%)与$CuSO_4$溶液(0.05 mol/L)按照体积比160∶40制备配位水凝胶,记为SC。按CP/SC比例1∶1、1∶2和2∶1,制备CPSC双网络水凝胶(n=3)。采用扫描电镜观察水凝胶的形貌,并用Image J测量其孔径。将干燥水凝胶称重(Wd)并测量计算总体积(Vt=长×宽×高)。将试样浸泡在乙醇中,并抽真空以确保液体完全浸入孔隙中。从乙醇中取出试样,擦去表面的液体,并迅速称重(Ws)。计算孔隙体积(Vp):$Vp=(Ws-Wd)/\rho l$,其中ρl是乙醇的密度,计算孔隙率(Φ)=Vp/Vt。

通过流变仪测定其机械性能,在1%剪应力

0.1 Hz下测试了水凝胶的储能模量(storage modulus,G′)和损耗模量(loss modulus,G″)。冻干样品浸泡在去离子水中直至平衡,并在不同时间点测试其重量变化($\Delta W = W - W_0$;W:吸水后重量;W_0:吸水前重量)。测量溶胀率为$W = \Delta W / W_0$。取冻干后的水凝胶应用衰减全反射法(attenuated total reflectance, ATR)进行傅里叶变换红外光谱(Fourier transform infrared spectroscopy,FTIR)检测。

1.3　双网络水凝胶-微针的制备及表征

分别配制3%(w/v)的透明质酸钠溶液和10%(w/v)的5-FU溶液。将1.5 mL的5-FU溶液和3.4 mL去离子水混匀,加入0.06%(w/v)的GNR溶液0.1 mL,加入透明质酸钠溶液5.0 mL,磁力搅拌1 h,配制为5-FU/GNR(5-fluorouracil/gold nanorod,FG)针尖预混液。取1 mL针尖预混液注入聚二甲基硅氧烷(polydimethylsiloxane,PDMS)模板中,真空3 min去除气泡,4 ℃静置8 h消泡。随后37 ℃干燥4 h,通过细胞刮刀除去多余的溶液,加入CPSC双网络水凝胶0.8 mL,填满PDMS模板。25 ℃干燥24 h,小心剥离得到双网络水凝胶-FG微针(简称FG微针)。制备5-FU与GNR针尖预混液,分别以去离子水替代上述配方中的GNR溶液或5-FU溶液,其余步骤相同,获得双网络水凝胶-5-FU微针(简称5-FU微针)和双网络水凝胶-GNR微针(简称GNR微针)。通过SEM观察FG微针的针尖形态。

将微针针尖朝上置于桌面,分别放置0、10、50、100、250、500 g砝码,静置5 min后体视显微镜下观察微针针尖变形情况测定力学性能。将4块FG微针分别刺入去除表面油脂等杂质后置于37 ℃恒温电热毯上的猪皮,0、15、30、60 min后取出,体式显微镜观察各时间点微针针尖变化探究溶解性能。使用万能材料试验机对FG微针(n=3)进行压缩测试,加载速度0.5 mm/min,记录载荷-位移曲线,并基于5%~15%应变区间的应力数据计算压缩模量。为了测量FG微针在常温和近红外光照射下5-FU的释放量,通过紫外分光光度法确定5-FU在265 nm处达到最大吸收峰,并绘制标准曲线。将FG微针置于PBS中透析,分为FG MN组(常温无处理)和FG MN+NIR组(分别于0、24、72和120 h行近红外光照射,0.4 W/cm^2,5 min/次)(n=3),2组持续透析7 d,测定5-FU的累积释放量。

1.4　双网络水凝胶-微针的光热性能表征

取1 mL GNR(9 μg/mL)溶液置于石英比色皿中,以808 nm的近红外光(0.4 W/cm^2)照射10 min至温度稳定,自然冷却10 min,每10 s记录温度。根据冷却曲线获得时间常数τ_s,依据Roper公式计算光热转换效率(η):

$$\eta = \frac{hS\left(T_{max} - T_{surr}\right) - Q_{Dis}}{I\left(1 - 10^{-A_{808}}\right)}$$

其中,h为传热系数,S为容器表面积,T_{max}为平衡温度,T_{surr}为环境温度,Q_{Dis}为溶剂吸热贡献,I为近红外光功率密度,A_{808}为GNR在808 nm处的吸光度。hS由冷却曲线线性拟合求得:

$$\tau_s = \frac{m_d C_d}{hS},\ \theta = \frac{T - T_{surr}}{T_{max} - T_{surr}},\ t = -\tau_s \ln\theta$$

采用3次循环照射(照5 min/停5 min)评估光热稳定性。另使用不同GNR浓度(0、3、6、9 μg/mL)的针尖预混液制备4组FG微针(n=3),以相同近红外光条件照射,每1 min记录温度并拍照,绘制循环温升曲线。

1.5　双网络水凝胶-微针细胞相容性实验

使用1.4制备的FG微针,经30 min紫外灭菌后,用含10%胎牛血清的DMEM培养基浸提24 h,经220 nm过滤器过滤得微针浸提液。将L929细胞(5.0×10^3个/孔)接种于96孔板,贴壁后更换为上述各组微针浸提液(n=3),培养48 h,加入含10% CCK-8试剂的培养基,孵育40 min后,通过酶标仪测定其在450 nm波长下的吸光度,计算细胞存活率,确定FG针尖预混液中GNR的浓度。

另取6 μg/mL GNR浓度的针尖预混液制备FG微针,用10%胎牛血清DMEM培养基配成100%浸提液,梯度稀释为50%、25%、10%、5%和0%:①以5.0×10个/孔分别将L929细胞和GMSM-K细胞接种于96孔板中,贴壁后换为上述浸提液(n=3),共培养2 d和4 d,CCK-8法检测细胞存活率;②将GMSM-K细胞接种于24孔板(8.0×10^3个/孔),贴壁后换为上述浸提液,共培养2 d和4 d后进行死/活细胞染色观察。

1.6　双网络水凝胶-微针的体外抗肿瘤实验

使用含0、0.5、1.5、3 mg/mL 5-FU的针尖预混液制备4组FG微针,同1.5方法灭菌、浸提,制备微针浸提液。将Cal-27细胞和L929细胞以5.0×10^3个/孔接种于96孔板中,贴壁后更换为上述各组微针浸提液(n=3)。共培养48 h,CCK-8法测定细胞存活率,确定FG针尖预混液中5-FU浓度。

实验分为Control组(完全培养基组),5-FU MN组(负载5-FU微针共培养组),GNR MN+NIR组(负载GNR微针共培养并接受0.4 W/cm^{2}的NIR照

射5 min组），FG MN+NIR组（负载5-FU和GNR微针共培养并接受相同NIR照射组）。所有微针均经30 min紫外灭菌，Cal-27细胞以8.0×10⁴个/孔的密度接种于24孔板，贴壁后通过Transwell小室与各组微针（n=3）：①共培养24 h和48 h后，CCK-8法测定细胞存活率；②共培养48 h后进行死/活细胞染色观察。

1.7　双网络水凝胶-微针的体内相容性评价和抗肿瘤及组织修复实验

本实验遵守动物研究指南：体内实验报告（The Animal Research：Reporting of In Vivo Experiments，ARRIVE）指南（https：//arriveguidelines.org），已获得四川大学华西口腔医院实验动物伦理委员会批准（审批号：WCHSIRB-D-2023-306）。根据预实验结果，选择12只健康雌性BALB/c-nu裸鼠，体重20~25 g。异氟烷麻醉后，皮下接种1×10⁶个/mL 100 μL Cal-27细胞悬液于左侧腋下。7 d后肿瘤体积达120~130 mm³，异氟烷麻醉进行手术切除大部分肿瘤（残留5%~10%体积）。随机数字法分为4组：Control组、5-FU MN组、GNR MN+NIR组和FG MN+NIR组，每组3只。Control组不做处理，其余组分别敷贴对应微针，GNR MN+NIR组和FG MN+NIR组进行NIR照射（0.4 W/cm²，5 min）。术后每3 d测量小鼠体重和肿瘤体积（V = 0.52 ×长×宽²），观察伤口愈合情况。14 d对裸鼠实施安乐死，完整切取复发肿瘤连同覆盖皮肤组织及心、肝、脾、肺、肾，4%多聚甲醛中固定24 h，脱水、透明后包埋切片，HE染色评估体内相容性和抗肿瘤效果。对复发肿瘤及皮肤组织Masson染色评估胶原沉积与创面愈合，免疫组化检测热休克蛋白70（heat shock protein 70，HSP70）和Ki-67蛋白（antigen Ki-67，Ki-67）表达水平。

1.8　统计学分析

使用GraphPad Prism 10软件进行统计分析，正态分布数据以均值±标准差表示，组间比较2组比较采用t检验，多组比较使用单因素方差分析及Tukey多重比较，P < 0.05为差异有统计学意义。

2　结　果

2.1　双网络水凝胶-微针的制备和表征

双网络水凝胶-微针的制备与表征如图1所示。由席夫碱水凝胶（CP）与配位水凝胶（SC）制备的CPSC双网络水凝胶具有多孔结构（图1a）。随着CP与SC配比的变化，双网络水凝胶的孔径增大，且孔隙度均能达到70%以上（图1b）。其中CP∶SC = 1∶1及CP∶SC = 1∶2的孔径在100~200 μm，这更加有利于细胞生长。CP∶SC = 2∶1的水凝胶G′低于200 Pa，而CP∶SC = 1∶1的水凝胶G′和G″均高于其他2组，且溶胀率最低（图1c、1d）。因此，CP∶SC = 1∶1的水凝胶具有更优的机械性能，更符合微针使用的设计要求，故选择该配比进行后续实验。如FTIR图谱所示，CPSC水凝胶在1 643 cm⁻¹处出现C=N产生的特征吸收峰，表明席夫碱键的存在（图1e）。

SEM图像显示，FG微针的针尖与背衬层连接部分能观察到明显分界，针尖呈四面椎体形（图1f），表明双层水凝胶-微针的成功制备。在10 g和50 g的砝码作用下，微针针尖保持完整无形变。在100~500 g砝码的作用力下，微针针尖发生弯折，但针体依然保持了完整结构未断裂，表明微针针尖具有较好的力学性能（图1g）。微针在刺入15 min后，针尖开始钝化，30 min后进一步溶解，刺入60 min后，针尖部分基本完全溶解（图1h）。微针的压缩测试显示，单根微针在发生断裂前的最大位移约为0.6 mm，能承受超过0.45 N的载荷，弹性模量为（1.69 ± 0.10）MPa（图1i、1j），足以确保微针有效穿透皮肤角质层并到达真皮层进行深层给药[16]。检测5-FU的最大吸收波长为265 nm，构建标准曲线Y = 0.045 74X - 0.018 26（R^2 = 0.999 2）（图1k、1l）。在首次近红外光照射后，FG MN+NIR组的5-FU释放率达到70.38% ± 2.49%（图1m）。在0~24 h内，FG MN+NIR组的5-FU释放率持续高于FG MN组，能够在肿瘤切除术后早期于局部形成高药物浓度，从而有效抑制残留肿瘤细胞的增殖与复发[17]。此外，FG微针的5-FU最终释放量为（851.47 ± 3.34）μg，低于1 mg（图1n），是相对安全的低剂量范围[18]。

2.2　双网络水凝胶-微针的光热性能表征

双网络水凝胶-微针的光热性能表征如图2所示。通过测定GNR溶液在808 nm的近红外光照射下的升温-冷却曲线，线性拟合得出时间常数τ_s为174.7，最终计算得到其光热转换效率η为31.4%（图2a、2b）。6 μg/mL的GNR针尖预混液制备的FG微针在近红外光照射5 min后温度达到48.4 ℃，符合杀伤肿瘤的温度（图2c、2d）。并且在3次循环光热过程中（图2e），FG微针表现出了稳定的光热性能。

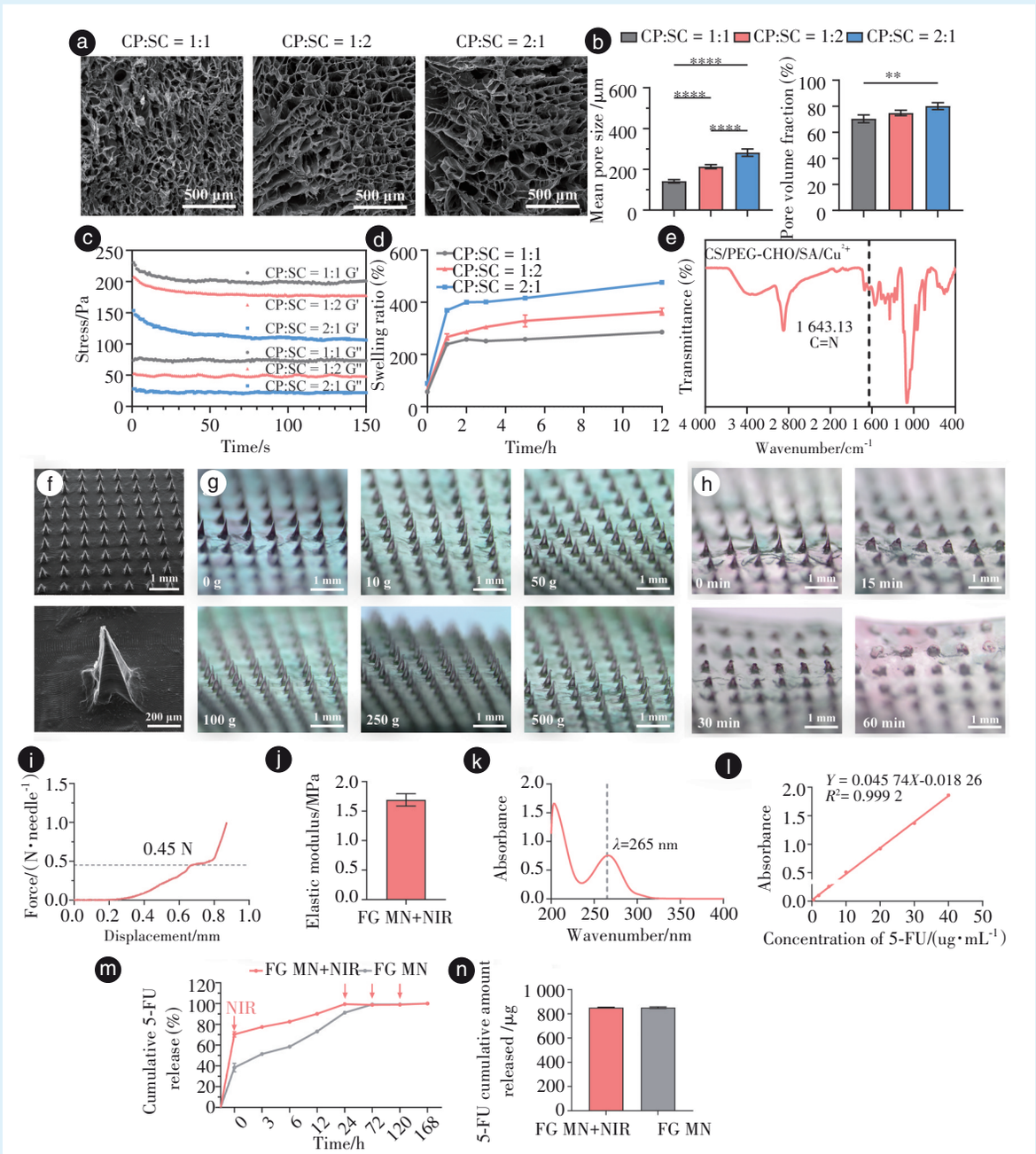

a: representative SEM images of hydrogels with chitosan/poly(ethylene glycol) dibenzaldehyde (CP):sodium alginate/Cu^{2+} (SC) ratios of 1:1, 1:2, and 2:1 show progressively increasing pore sizes. b: the smallest pore size and porosity were observed at a CP:SC ratio of 1:1. c & d: the highest storage modulus (G′) and loss modulus (G″) and the lowest swelling ratio were achieved at a CP:SC ratio of 1:1. e: the characteristic absorption peak of the C=N bond was at 1 643 cm^{-1}. f: representative images showing 5-fluorouracil/gold nanorod (FG) microneedles with a tetrahedral pyramidal structure and distinct interface. g: representative images showing FG microneedles bending yet remaining structural integrity under a 500 g load. h: representative images showing near-complete dissolution of needle tips after 60 min. i: mechanical properties of a single microneedle, showing a maximum displacement of −0.6 mm before fracture and the ability to withstand a load exceeding 0.45 N. j: the elastic modulus was (1.69 ± 0.10) MPa. k: ultraviolet-visible absorption spectrum of 5-fluorouracil (5-FU) showing a maximum absorption wavelength (λ) at 265 nm. l: standard calibration curve of 5-FU. m: the release rate of 5-FU from the FG MN + NIR group was higher than that of the FG MN group during the first 24 h. n: release at 168 h; no significant difference between groups. FG MN: FG microneedles stored at room temperature without any treatment; FG MN + NIR: FG microneedles irradiated with near-infrared (NIR) light (0.4 W/cm^2, 808 nm, 5 min) at 0, 24, 72, and 120 h. All experiments above: n=3. Statistical analysis used t-test for two groups or one-way ANOVA with Tukey's test for multiple groups. $^{**}P < 0.01$, $^{****}P < 0.000\ 1$

Figure 1　Preparation and characterization of the dual-network hydrogel-microneedle

图1　双网络水凝胶-微针的制备与表征

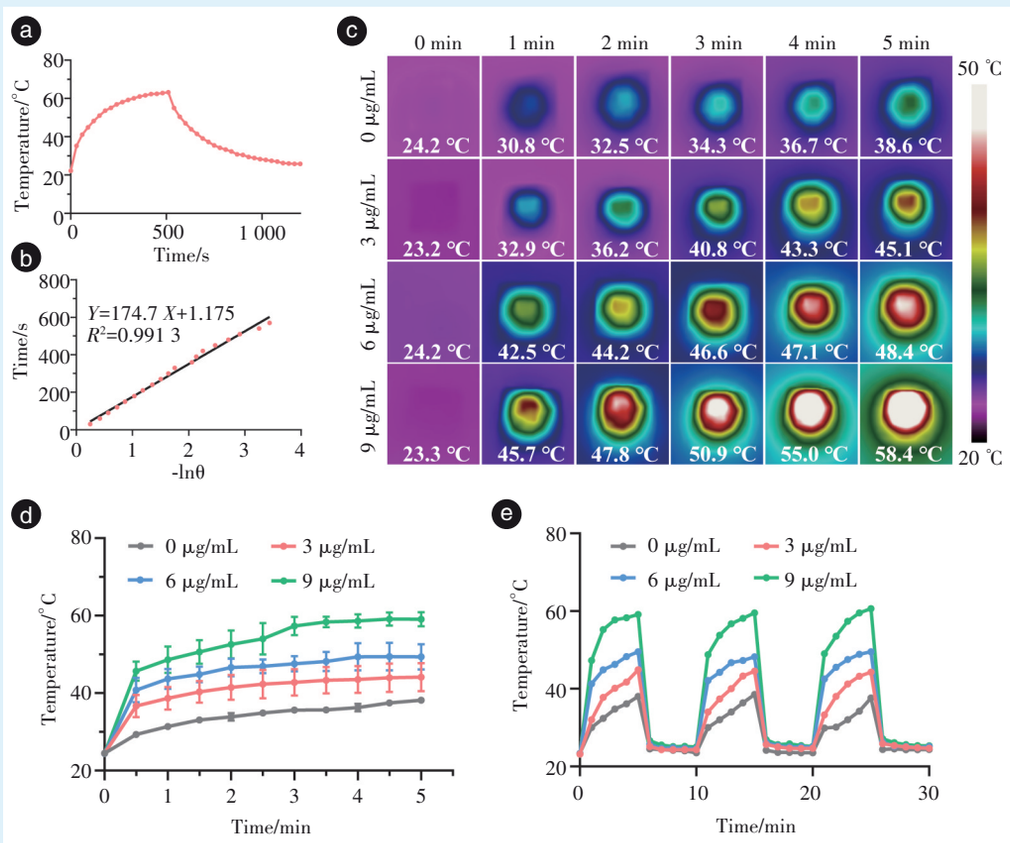

a: heating-cooling curve of the gold nanorod (GNR) solution at 9 μg/mL. b: time constant τ_s of 174.7 and photothermal conversion efficiency (η) of 31.4% calculated from the linear fit of lnθ-time during the GNR cooling stage. c: representative results show that, after 5 min of near-infrared (NIR) irradiation, 5-fluorouracil/gold nanorod (FG) microneedles prepared from tip-premixed GNR solutions at concentrations of 0, 3, 6, and 9 μg/mL reached temperatures of 38.6° C, 45.1° C, 48.4° C, and 58.4° C, respectively. d: the final temperature achieved by the 6 μg/mL FG microneedle group better met the requirement for photothermal tumor ablation while offering improved biosafety compared with the 9 μg/mL group. e: the heating curves of FG microneedles overlapped stably over three consecutive heating-cooling cycles. 0 μg/mL: FG microneedles without GNR. 3, 6, 9 μg/mL: FG microneedles prepared from tip-premixed GNR solutions at 3, 6, and 9 μg/mL. NIR irradiation parameters: 0.4 W/cm^2, 808 nm. All experiments above: n=3

Figure 2　Photothermal performance characterization of the dual-network hydrogel-microneedle

图2　双网络水凝胶-微针的光热性能表征

2.3　双网络水凝胶-微针细胞相容性评价

双网络水凝胶-微针细胞相容性评价如图3所示。CCK-8检测结果显示，9 μg/mL GNR针尖预混液制备的FG微针组L929细胞活力低于70%。0~6 μg/mL的3组细胞活力均保持在90%以上（图3a）。为兼顾光热转换效率与生物安全性，本研究最终选定以6 μg/mL GNR针尖预混液制备的FG微针进行后续实验。

各浓度组FG微针浸提液在培养L929细胞24 h和48 h后，细胞活力均高于90%（图3b）。在共培养4 d后，FG MN组的L929细胞活力高于Control组，差异具有统计学意义（P < 0.000 1）（图3c）。

FG MN组的GMSM-K细胞在培养2 d和4 d后，细胞活力高于Control组（图3d）。死/活细胞染色结果进一步直观显示（图3e），FG MN组在共培养2 d和4 d后绿色荧光（活细胞）密度高于Control组，几乎未见红色荧光（死细胞）。上述结果表明，FG微针不仅无细胞毒性，还展现出优异的促进细胞增殖的潜力，展现出良好的临床应用前景。

2.4　双网络水凝胶-微针体外抗肿瘤效果评价

双网络水凝胶-微针体外抗肿瘤效果评价如图4所示。

CCK-8检测结果显示，随着制备FG微针的针尖预混液中5-FU浓度的升高，共培养的Cal-27细胞活力下降（图4a）。0.5 mg/mL与1.5 mg/mL组的L929细胞共培养后细胞活力高于90%，但3.0 mg/mL组细胞活力低于80%。1.5 mg/mL组在抑制Cal-27活性的同时，对L929细胞毒性较低。因此最终以1.5 mg/mL 5-FU针尖预混液制备的FG微针进行后续实验。

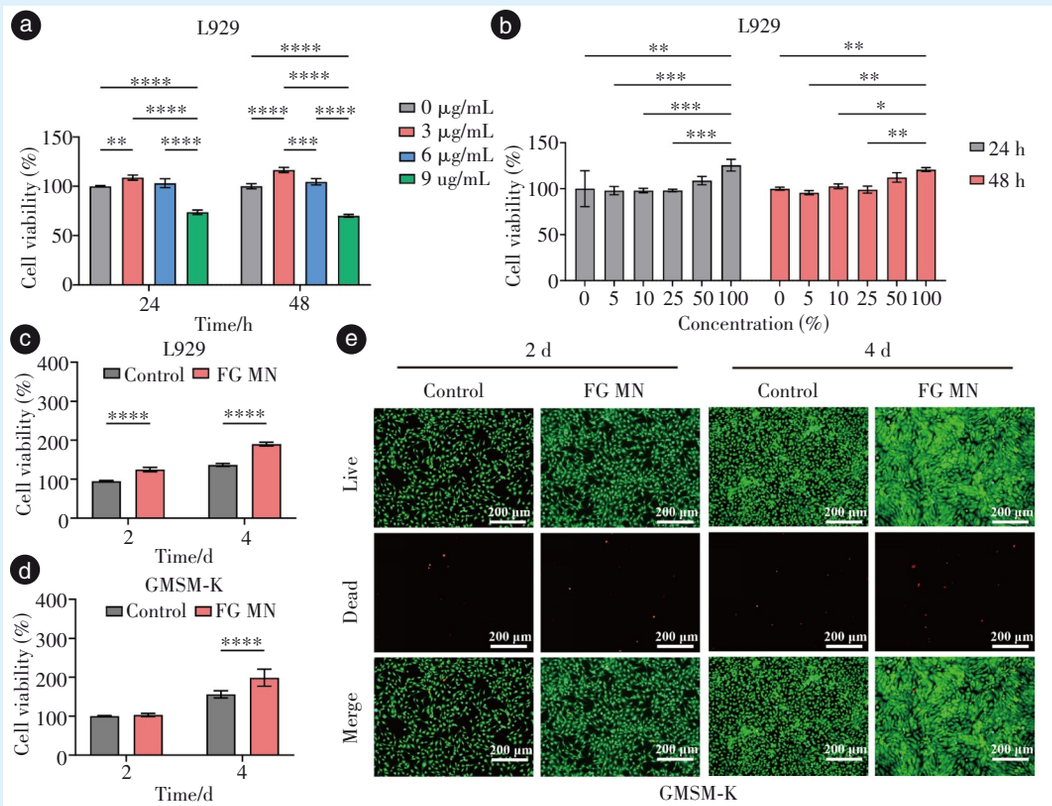

a: L929 cell viability remained above 90% when co-cultured with 5-fluorouracil/gold nanorod (FG) microneedles prepared from tip-premixed gold nanorod (GNR) solutions at concentrations of 0-6 μg/mL, but decreased to below 70% with the 9 μg/mL group. b: L929 cells exhibited viabilities above 90% after 24 h and 48 h of co-culture with FG microneedles at extract concentrations of 0%, 5%, 10%, 25%, 50%, and 100%. c: L929 cell viability in the FG MN group was significantly higher than that in the control group after 2 and 4 days of co-culture. d: GMSM-K cell viability in the FG MN group was significantly higher than that in the control group after 2 and 4 days of co-culture. e: representative images showing higher live cell density (green fluorescence) in the FG MN group versus the control group after 2 and 4 days of co-culture. Control group: complete culture medium group. FG MN group: FG microneedles co-cultured with cells. All experiments above: n=3. Statistical analysis used t-test for two groups or one-way ANOVA with Tukey's test for multiple groups. *P < 0.05. **P < 0.01. ***P < 0.001.**** P < 0.000 1

Figure 3　*In vitro* cytocompatibility of the dual-network hydrogel-microneedle with L929 and GMSM-K cells

图3　双网络水凝胶-微针对L929和GMSM-K细胞的体外相容性评价

CCK-8检测结果如图4b所示，共培养24 h后Control组的Cal-27细胞活力最高，5-FU MN组的细胞活力降为96.3%，GNR MN+NIR组的细胞活力降为90.8%，FG MN+NIR组细胞活力降低至79.0%。共培养48 h后Cal-27细胞活力进一步降低，5-FU MN组细胞活力为16.3%，GNR MN+NIR组细胞活力为5.4%，而FG MN+NIR组细胞活力仅为1.0%。化疗药物与光热治疗联合的FG MN+NIR组表现出更强地抑制Cal-27细胞增殖的效果。

如图4c的死/活细胞染色显示，Control组以明亮的绿色荧光（活细胞）为主，5-FU MN组和GNR MN+NIR组中均观察到部分的红色荧光（死细胞），但仍有大量Cal-27细胞存活。相比之下，FG MN+NIR组中出现大面积和高密度的红色荧光，仅存极少量的绿色荧光。化疗-光热联合治疗的FG MN+NIR组相较于其他3组，更有效地诱导了Cal-27细胞死亡。

2.5　双网络水凝胶-微针体内生物相容性评价

双网络水凝胶-微针体内生物相容性评价如图5所示。HE染色结果显示，与Control组相比，各组微针皮下植入裸鼠7 d后，主要脏器形态结构正常，未观察到明显的炎症细胞浸润，组织坏死或病变，表明本研究的FG微针具有良好的体内生物安全性。

2.6　双网络水凝胶-微针体内抗肿瘤复发效果评价

双网络水凝胶-微针体内抗肿瘤复发效果评价如图6所示。Cal-27细胞皮下接种7 d后，各组裸鼠肿瘤体积达（122.70±3.56）mm^3，差异无统计学意义，表明造模成功（图6a~6c）。热成像显示，FG MN+NIR组在近红外光照射5 min下，肿瘤创面局部温度升至48.2 ℃，达到杀灭肿瘤的温度（图6d）。

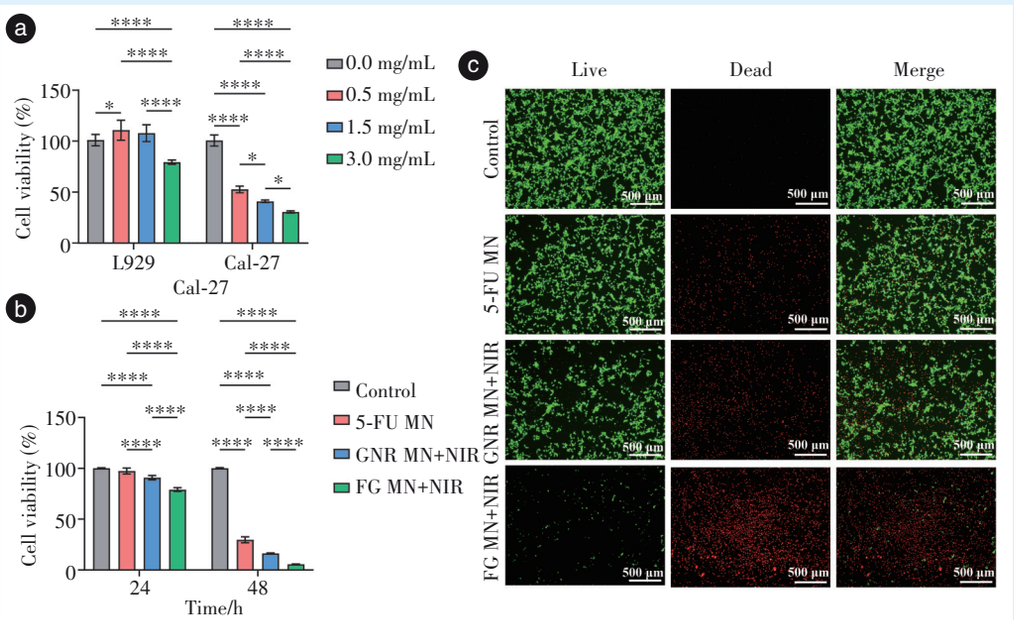

a: the 1.5 mg/mL group effectively suppressed Cal-27 cell viability while exhibiting low cytotoxicity toward L929 cells. 0.0 mg/mL: 5-fluorouracil/gold nanorod (FG) microneedle without 5-fluorouracil (5-FU). 0.5, 1.5, and 3.0 mg/mL: FG microneedle prepared from tip-premixed 5-FU solutions at 0.5, 1.5, and 3.0 mg/mL. b: compared with control group, Cal-27 cell viability was lower in the 5-FU MN and gold nanorod (GNR) MN + NIR groups, and the FG MN + NIR group showed the lowest viability. c: representative images showing mainly green fluorescence (live cells) in the control group, red fluorescence (dead cells) in the 5 FU MN and GNR MN + NIR groups, and extensive red signals in the FG MN + NIR group. Control group: complete culture medium group. 5-FU MN group: microneedles loaded with 5-FU, co-cultured with cells. GNR MN + NIR group: microneedles loaded with GNR, co-cultured with cells and exposed to near-infrared (NIR) irradiation. FG MN + NIR group: microneedles co-loaded with 5-FU and GNR, co-cultured with cells and exposed to NIR irradiation. All experiments above: n =3. Statistical analysis used one-way ANOVA with Tukey's test for multiple groups. *P < 0.05, ****P < 0.000 1

Figure 4　*In vitro* anti-tumor efficacy of the dual-network hydrogel-microneedle against Cal-27 cells

图4　双网络水凝胶-微针对Cal-27细胞的体外抗肿瘤效果评价

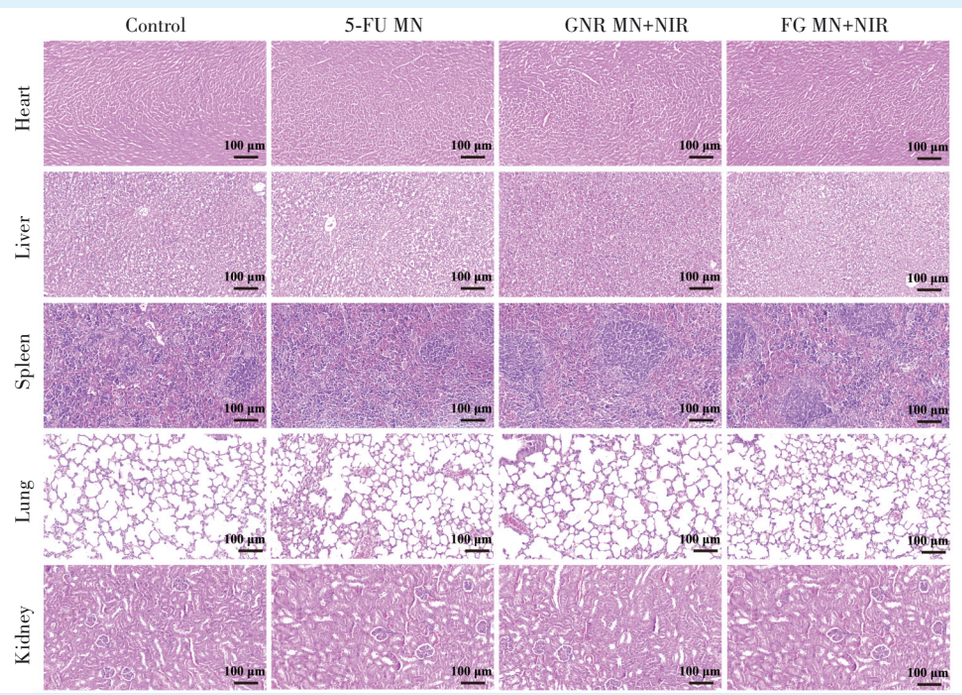

Representative images showing major organs retained normal histological architecture with no obvious inflammation at day 7 post-implantation. Control: control group. 5-FU MN: animals treated with 5-fluorouracil (5-FU) -loaded microneedles. GNR MN + NIR: animals treated with gold nanorod (GNR) -loaded microneedles followed by near-infrared (NIR) irradiation. FG MN + NIR: animals treated with microneedles co-loaded with 5-FU and GNR, followed by NIR irradiation. n=3 mice

Figure 5　*In vivo* biocompatibility of the dual-network hydrogel-microneedle in BALB/c nude mice

图5　双网络水凝胶-微针在BALB/c-nu裸鼠体内相容性评价

肿瘤切除术后14 d，Control组的肿瘤持续增长，体积达（380.93±44.30）mm^3。5-FU MN组和GNR MN+NIR组对肿瘤复发均有一定的抑制作用，肿瘤体积分别为（180.42 ± 5.23）mm^{3}和（82.04 ± 10.32）mm^3（图6e、6f）。FG MN+NIR组的几乎未见明显肿瘤复发，体积仅（2.50 ± 4.32）mm^3，同时该组裸鼠体重也呈稳定上升趋势（图6g）。

免疫组化分析显示，GNR MN+NIR组和FG MN+NIR组中，HSP70表达均升高，且FG MN+NIR组的HSP70的表达量更高（图6h~6j）。与此同时，Ki-67染色结果显示，联合治疗组的Ki-67阳性率低于其余组，差异具有统计学意义（$P < 0.000\ 1$），有效地抑制了肿瘤细胞增殖。综上，化疗-光热联合治疗不仅通过热应激直接杀伤肿瘤细胞，还增强了5-FU的抗肿瘤效应，实现了最优的抑制OSCC肿瘤复发效果。

2.7　双网络水凝胶-微针促进组织修复效果评价

双网络水凝胶-微针促进组织修复效果评价见图7。术后14 d，Control组的创面仍未完全修复，表面有大片血痂。微针治疗的3组裸鼠皮肤创面的修复速度均高于Control组，表面几乎没有大面积明显创面（图7a、7b）。尤其以FG MN+NIR组的创面残留率最低，仅0.44% ± 0.73%，组织愈合情况最佳。结合HE染色的组织学分析显示（图7c、7d），Control组的皮肤组织内可见大量聚集的肿瘤细胞。相比之下，5-FU MN组和GNR MN+NIR组中肿瘤细胞减少，但仍有部分肿瘤细胞残留，FG MN+NIR组的几乎无肿瘤细胞残留。Masson染色结果（图7e、7f）显示，Control组中的肿瘤间质内存在紊乱的病理性胶原沉积，5-FU MN组和GNR MN+NIR组随着肿瘤消退，病理性胶原面积随之减少。在FG MN+NIR组中，病理性胶原沉积基本消失，出现大量排列有序、结构连续的新生胶原纤维，标志着真皮层的有效重建。上述结果表明，化疗-光热联合治疗高效地清除了肿瘤并促进了组织再生。

3　讨　论

3.1　减毒增效的局部药物递送

本研究构建的双网络水凝胶-微针，通过联合局部化疗和光热治疗，为OSCC术后复发防治提供了一种创新策略。传统治疗模式下，全身化疗的毒性风险[19]与局部药物递送效率不足[20]是制约疗效的关键因素，而手术切除后残留的微小病灶及缺氧、免疫抑制[21]等肿瘤微环境的异常会进一步加剧复发风险。本研究中，微针的局部精准给药特性能够提升5-FU在肿瘤部位的富集[22-23]。结合体外药物释放及体内抗肿瘤实验共同证实，该体系的5-FU总释放量低于1 mg，但在Cal-27源性皮下OSCC术后复发模型中，有效抑制了肿瘤的复发，并加速促进了创面愈合。相较于传统注射或口服给药，这种减毒增效的模式更符合临床对安全性及疗效的双重需求[24-25]。

3.2　化疗与光热治疗的协同

OSCC术后光热治疗与化疗的协同效应是本研究的核心创新点。体外Cal-27细胞的CCK-8及死/活细胞染色实验，结合体内肿瘤治疗结果，证实了化疗-光热联合治疗实现了高效的抑制OSCC复发效果。肿瘤组织的免疫组化分析进一步揭示了其潜在机制，FG MN+NIR组中HSP70的表达上调，Ki-67的表达则大幅降低。这表明，光热疗法不仅通过局部高热直接诱导肿瘤细胞产生热损伤与坏死[26-27]，更关键的是通过上调HSP70引发强烈的热应激反应[28]，从而增强了化疗药物的疗效[29-30]。相比之下，5-FU MN组和GNR MN+NIR组的Ki-67阳性率均高于FG MN+NIR组，这一差异有力证实了光热治疗与化疗的协同抑制OSCC复发的效应。

针对化疗药物释放快，难以清除深层肿瘤部位的难题[31]。本研究设计利用微针的穿透深度优势，能够突破口腔黏膜屏障，将药物直接递送至深层肿瘤组织，有效克服了传统化疗表面给药难以渗透的局限性[32-33]。同时在微针局部给药后即刻进行近红外照射，在初期实现高浓度快速释放，在光热治疗辅助治疗的同时，确保肿瘤部位能维持有效的药物浓度，最大化地抑制了肿瘤细胞增殖[34]。当5-FU释放进入平台期后，通过多次近红外照射诱导的热应激，进一步调控并抑制了残留肿瘤细胞的活性。这种早期高浓度化疗协同热疗杀伤，后期多次热疗维持抑制复发的治疗模式，不仅弥补了单纯化疗药物清除快和后期药效不足的缺陷，也解决了单独热疗效果不佳的局限[35]。对肿瘤的高效清除，术后创面也呈现出良好的愈合效果，体现了该体系在抑制OSCC复发治疗及后续修复的临床应用潜力[36-37]。

3.3　总结与展望

本研究仍存在一定的局限性。基于OSCC术后复发高峰通常出现在2~3周内，并参考同类局部治疗研究的观察周期[38-39]，本研究设计了14 d的观

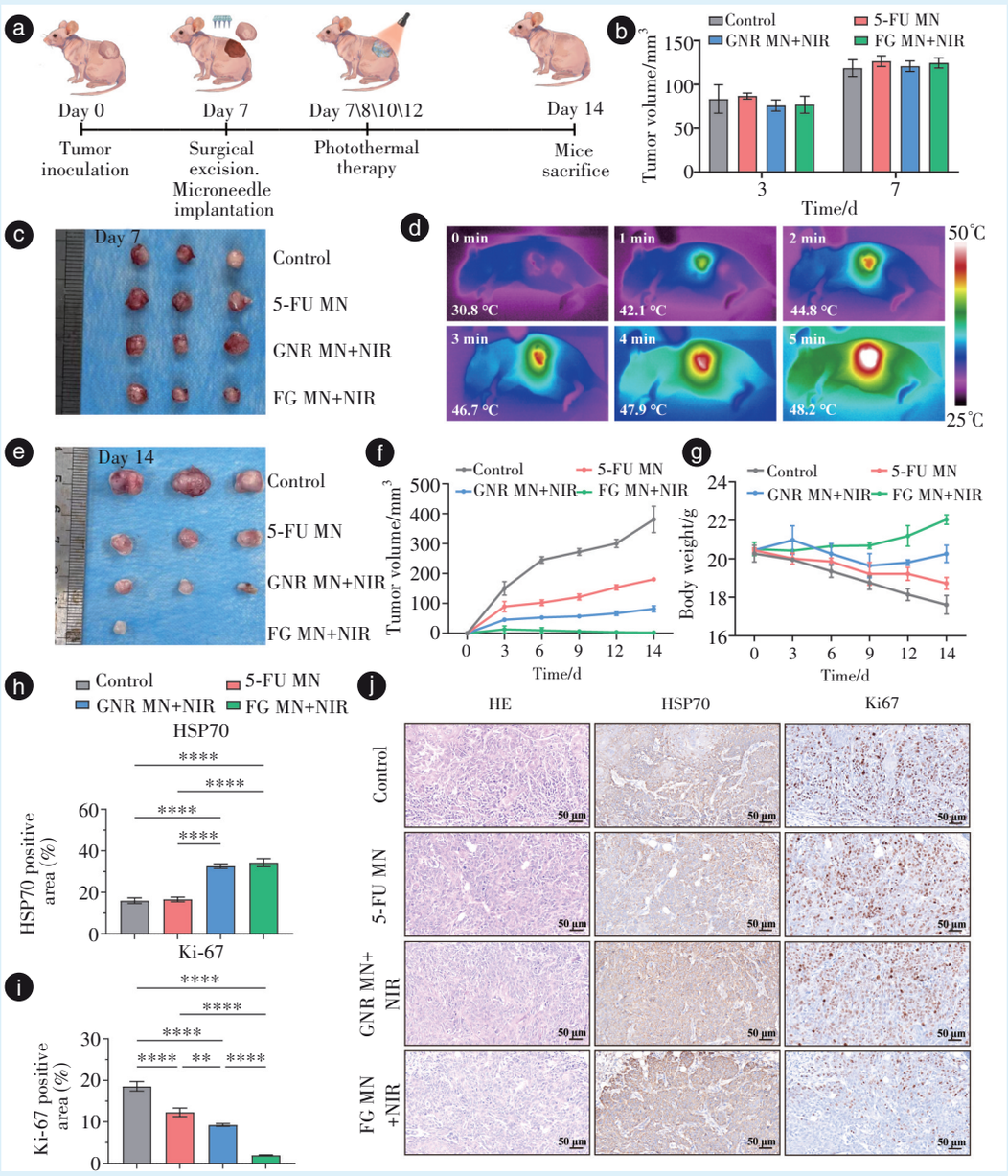

a: schematic of oral squamous cell carcinoma (OSCC) postoperative recurrence model establishment and therapeutic regimen. b: tumor volumes at 3 and 7 days after Cal-27 cell inoculation showed no statistical difference among groups. c: excised tumors at postoperative day 7 were uniform in size across all groups. d: in the FG MN + NIR group, local tumor temperature rapidly increased to 48.2°C within 5 min of near-infrared (NIR) irradiation. e: at postoperative day 14, recurrent tumors resected from the FG MN + NIR group were smaller than those from all other groups, with some even absent. f: from postoperative days 0 to 14, tumor volume in the control group progressively increased due to recurrence, whereas the 5-FU MN and GNR MN + NIR groups exhibited mild recurrence, and the FG MN + NIR group consistently maintained the lowest tumor volume. g: during days 0-14 post-surgery, the body weight of mice in the control group gradually declined, showed slight fluctuations in the 5-FU MN and GNR MN + NIR groups, and steadily increased in the FG MN+NIR group. h: the FG MN + NIR group exhibited the highest heat shock protein 70 (HSP70)-positive rate among all groups. i: the FG MN + NIR group exhibited the lowest antigen Ki-67 (Ki-67)-positive rate among all groups. j: representative images showing the strongest HSP70 and weakest Ki-67 immunostaining signals in the FG MN + NIR group. Control: control group. 5-FU MN: animals treated with 5-fluorouracil (5-FU)-loaded microneedles. GNR MN + NIR: animals treated with gold nanorod (GNR)-loaded microneedles followed by NIR irradiation. FG MN + NIR: animals treated with microneedles co-loaded with 5-FU and GNR, followed by NIR irradiation. All experiments above: n=3. Statistical analysis used one-way ANOVA with Tukey's test for multiple groups. $^{**}P < 0.01$, $^{****}P < 0.000\ 1$

Figure 6　Anti-tumor recurrence efficacy of the dual-network hydrogel-microneedle in a subcutaneous Cal-27-derived oral squamous cell carcinoma post-surgical recurrence model in BALB/c nude mice

图6　网络水凝胶-微针在Cal-27源性皮下OSCC术后复发BALB/c-nu裸鼠模型中抗肿瘤复发效果评价

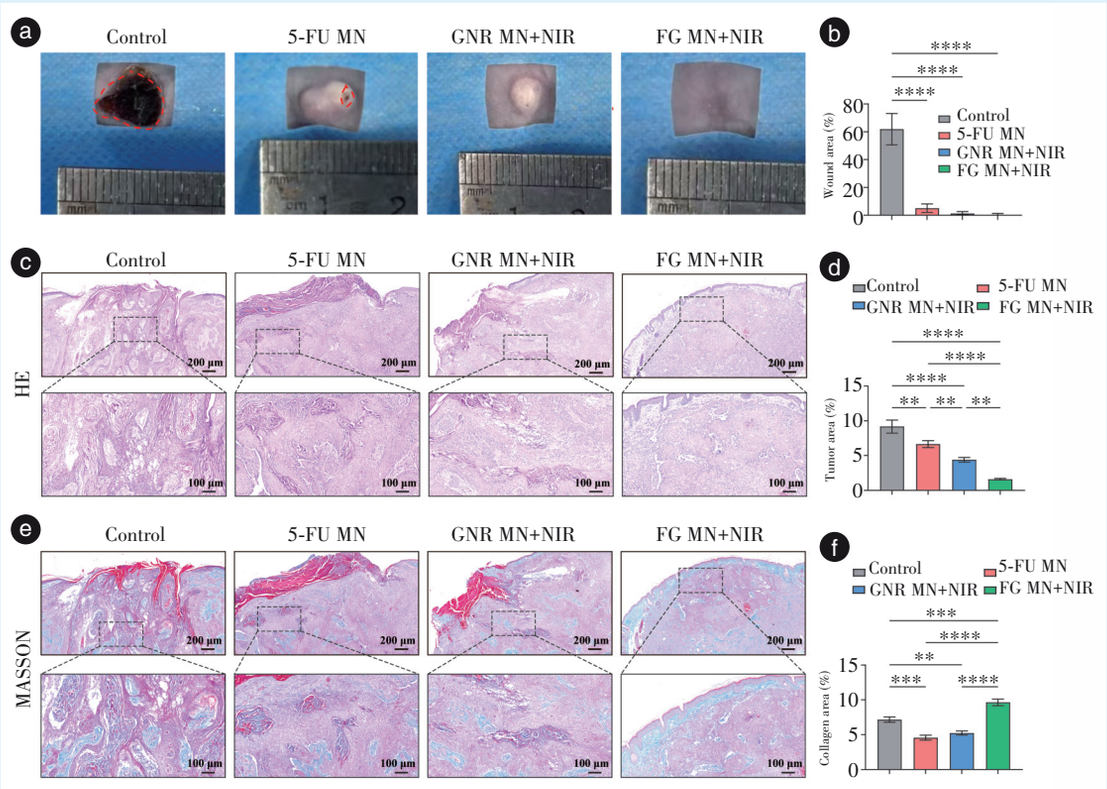

a: representative results show near-complete healing in the FG MN + NIR group versus other groups (red dashed lines: unhealed areas). b: wound residual rate in the FG MN + NIR group was only 0.44% ± 0.73%, lower than that of the other groups. c: representative results show only minimal residual tumor cells in the FG MN + NIR group. d: the area of residual tumor cells was smaller in the FG MN + NIR group compared to other groups. e: representative results show largely absent pathological collagen in the FG MN + NIR, with abundant newly formed, well organized fibers. f: the collagen deposition area was greater in the FG MN + NIR group than in other groups. Control: control group. 5-FU MN: animals treated with 5-fluorouracil (5-FU)-loaded microneedles. GNR MN + NIR: animals treated with gold nanorod (GNR)-loaded microneedles followed by near-infrared (NIR) irradiation. FG MN + NIR: animals treated with microneedles co-loaded with 5-FU and GNR, followed by NIR irradiation. All experiments above: n=3. Statistical analysis used one-way ANOVA with Tukey's test for multiple groups. $^{**}P < 0.01$, $^{***}P < 0.001$, $^{****}P < 0.000\ 1$

Figure 7　Tissue repair efficacy of the dual-network hydrogel-microneedle on day 14 in a subcutaneous Cal-27-derived oral squamous cell carcinoma post-surgical recurrence model in BALB/c nude mice

图7　双网络水凝胶-微针在Cal-27源性皮下OSCC术后复发BALB/c-nu裸鼠模型中14 d组织修复效果评价

察窗口以初步评估术后早期的肿瘤复发情况。然而,14 d的观察期尚不足以全面评估长期疗效及远期复发风险,需延长实验周期以验证其长效抗肿瘤能力。为遵循动物实验伦理的3R原则,本研究体内实验每组设置的3个重复样本量偏小,尽管统计学分析显示组间差异具有统计学意义,但难以全面反映个体差异对疗效的影响。因此,未来研究亟需扩大动物样本量,以验证该体系在不同个体间的稳定性与可重复性。虽然治疗期间小鼠体重稳定且主要器官组织学未见明显病理改变,但本研究尚未对5-FU和GNR在体内的长期代谢和毒性进行系统评估,缺乏血液生化指标的动态监测数据,未来需开展更全面的毒理学研究以确立其临床转化安全性。同时,考虑到真实口腔环境具有湿润、动态及唾液冲刷等复杂特点[40-42],本研究体系的粘附稳定性、长效释药行为仍有待在更接近临床的大动物模型中进行深入验证。尽管存在上述挑战,本研究构建的双网络水凝胶-微针通过微针微创给药降低了5-FU的全身毒性风险,同时实现了局部化疗与光热治疗的有效整合,为抑制OSCC的复发治疗提供了新的研究思路和理论参考。

【Author contributions】 Chu MX performed the experiments, analyzed the data and wrote the article. Ye XW, Xie X analyzed the data and revised the article. Liao JF designed the study and revised the article. All authors read and approved the final manuscript as submitted.

【Ethics Statement】 All animal procedures were carried out in compliance with the ARRIVE guidelines (https://arriveguidelines.org) and adhered to the guidelines for the care and use of laboratory animals issued by the China Animal Research Council. All animal experiments were approved by Experimental Animal Ethics Committee of West China Hospital of Stomatology, Sichuan University (Approval ID: WCHSIRB-D-2023-306).

【Funding】 This study was supported by the grants from National Natural Science Foundation of China (No. 32171354). The funder had no role in the study design, data collection and analysis, decision to publish, or preparation of the manuscript.

【Competing interests】 All authors have completed the ICMJE uniform disclosure form at www.icmje.org/disclosure-of-interest/ and declare: support from the National Natural Science Foundation of China (No. 32171354) for the submitted work; no financial relationships with any organisations that might have an interest in the submitted work in the previous three years; no other relationships or activities that could appear to have influenced the submitted work.

【Data availability statement】 The original contributions presented in this study are included in the article. Further inquiries can be directed to the corresponding author upon reasonable request.

【Generative AI statement】 The authors declared that generative AI was not used in the creation of this manuscript.

参考文献

[1] Panarese I, Aquino G, Ronchi A, et al. Oral and oropharyngeal squamous cell carcinoma: prognostic and predictive parameters in the etiopathogenetic route[J]. Expert Rev Anticancer Ther, 2019, 19(2): 105-119. doi: 10.1080/14737140.2019.1561288.

[2] Johnson DE, Burtness B, Leemans CR, et al. Head and neck squamous cell carcinoma[J]. Nat Rev Dis Primers, 2020, 6(1): 92. doi: 10.1038/s41572-020-00224-3.

[3] de Baco LS, da Silva LC, Antunes LCM, et al. Evaluation of chemotherapy toxicities in patients receiving treatment for gastrointestinal cancers and therapeutic monitoring of 5-fluorouracil as a clinical support tool[J]. Fundam Clin Pharmacol, 2024, 38(6): 1190-1202. doi: 10.1111/fcp.13037.

[4] Li N, Wang Y, Wang A, et al. STS1 and STS2 phosphatase inhibitor baicalein enhances the expansion of hematopoietic and progenitor stem cells and alleviates 5-fluorouracil-induced myelosuppression[J]. Int J Mol Sci, 2023, 24(3): 2987. doi: 10.3390/ijms24032987.

[5] Sobol NT, Solerno LM, Llavona C, et al. Vasopressin analog [V^4Q^5] dDAVP exerts cooperative anticancer effects in combination with low-dose 5-fluorouracil on aggressive colorectal cancer models[J]. World J Oncol, 2023, 14(6): 540-550. doi: 10.14740/wjon1715.

[6] Deng YN, Chen Y, Gao S, et al. RREB1-mediated SUMOylation enhancement promotes chemoresistance partially by transcriptionally upregulating UBC9 in colorectal cancer[J]. Front Pharmacol, 2024, 15: 1381860. doi: 10.3389/fphar.2024.1381860.

[7] Danella EB, Costa de Medeiros M, D'Silva NJ. Cytokines secreted by inflamed oral mucosa: implications for oral cancer progression [J]. Oncogene, 2023, 42(15): 1159-1165. doi: 10.1038/s41388-023-02649-y.

[8] Maurya S, Prasad D, Mukherjee S. Matrix metalloproteinases in oral cancer pathogenesis and their use in therapy[J]. Anticancer Agents Med Chem, 2024, 24(1): 3-17. doi: 10.2174/0118715206270002231108071917.

[9] Buruiană A, Gheban BA, Gheban-Ro ca IA, et al. The tumor stroma of squamous cell carcinoma: a complex environment that fuels cancer progression[J]. Cancers, 2024, 16(9): 1727. doi: 10.3390/cancers16091727.

[10] Ahmed Saeed Al-Japairai K, Mahmood S, Hamed Almurisi S, et al. Current trends in polymer microneedle for transdermal drug delivery[J]. Int J Pharm, 2020, 587: 119673. doi: 10.1016/j.ijpharm.2020.119673.

[11] Wang S, Zhao M, Yan Y, et al. Flexible monitoring, diagnosis, and therapy by microneedles with versatile materials and devices toward multifunction scope[J]. Research, 2023, 6: 0128. doi: 10.34133/research.0128.

[12] Shao J, Li X, Li Y, et al. Self-heating multistage microneedle patch for topical therapy of skin cancer[J]. Adv Mater, 2024, 36(15): e2308217. doi: 10.1002/adma.202308217.

[13] Fang S, Lin J, Li C, et al. Dual-stimuli responsive nanotheranostics for multimodal imaging guided trimodal synergistic therapy[J]. Small, 2017, 13(6): 1602580. doi: 10.1002/smll.201602580.

[14] Li Q, Hou Y, Sun D, et al. Natural protein-based multifunctional hydrogel dressing formed by rapid photocuring and zinc ion coordination to accelerate wound healing[J]. ACS Appl Mater Interfaces, 2025, 17(4): 5719-5734. doi: 10.1021/acsami.4c16083.

[15] Chen Z, Zhou Z, Zhang X, et al. A carboxymethyl chitosan and dextran hydrogel with slow and rapid photothermal conversion for sequential promoting burn wound healing and inhibiting scar proliferation[J]. Carbohydr Polym, 2025, 350: 123045. doi: 10.1016/j.carbpol.2024.123045.

[16] Zhou R, Yu H, Sheng T, et al. Grooved microneedle patch augments adoptive T cell therapy against solid tumors *via* diverting regulatory T cells[J]. Adv Mater, 2024, 36(30): e2401667. doi: 10.1002/adma.202401667.

[17] Zhu Z, Wang J, Pei X, et al. Blue-ringed octopus-inspired microneedle patch for robust tissue surface adhesion and active injection drug delivery[J]. Sci Adv, 2023, 9(25): eadh2213. doi: 10.1126/sciadv.adh2213.

[18] Yang ZR, Suo H, Fan JW, et al. Endogenous stimuli-responsive separating microneedles to inhibit hypertrophic scar through remodeling the pathological microenvironment[J]. Nat Commun, 2024, 15(1): 2038. doi: 10.1038/s41467-024-46328-2.

[19] Goldberg M, Manzi A, Birdi A, et al. A nanoengineered topical transmucosal cisplatin delivery system induces anti-tumor response in animal models and patients with oral cancer[J]. Nat Commun, 2022, 13(1): 4829. doi: 10.1038/s41467-022-31859-3.

[20] Elsaady SA, Aboushelib MN, Al-Wakeel E, et al. A novel intratumoral drug delivery carrier for treatment of oral squamous cell carcinoma[J]. Sci Rep, 2023, 13(1): 11984. doi: 10.1038/s41598-023-38230-6.

[21] Liang Y, Bu Q, You W, et al. Single-cell analysis reveals hypoxia-induced immunosuppressive microenvironment in intrahepatic cholangiocarcinoma[J]. Biochim Biophys Acta Mol Basis Dis, 2024, 1870(7): 167276. doi: 10.1016/j.bbadis.2024.167276.

[22] Li P, Liu CH, Zhao YY, et al. Multifunctional covalent organic framework-based microneedle patch for melanoma treatment[J]. Biomacromolecules, 2023, 24(8): 3846-3857. doi: 10.1021/acs.biomac.3c00488.

[23] Ziesmer J, Sondén I, Thersleff T, et al. Highly efficient near-IR photothermal microneedles with flame-made plasmonic nanoaggregates for reduced intradermal nanoparticle deposition[J]. Adv Mater Interfaces, 2022, 9(34): admi. 202201540. doi: 10.1002/admi.202201540.

[24] Suriyaamporn P, Pornpitchanarong C, Charoenying T, et al. Artificial intelligence-driven hydrogel microneedle patches integrating 5-fluorouracil inclusion complex-loaded flexible pegylated liposomes for enhanced non-melanoma skin cancer treatment[J]. Int J Pharm, 2025, 669: 125072. doi: 10.1016/j.ijpharm.2024.125072.

[25] Cao J, Wu B, Yuan P, et al. Advances in research of hydrogel microneedle-based delivery systems for disease treatment[J]. Pharmaceutics, 2024, 16(12): 1571. doi: 10.3390/pharmaceutics16121571.

[26] Qi MH, Wang DD, Qian W, et al. High-efficiency gold nanoaggregates for NIR LED-driven sustained mild photothermal therapy achieving complete tumor eradication and immune enhancement [J]. Adv Mater, 2025, 37(5): e2412191. doi: 10.1002/adma.202412191.

[27] Liu S, Pan X, Liu H. Two-dimensional nanomaterials for photothermal therapy[J]. Angew Chem Int Ed Engl, 2020, 59(15): 5890-5900. doi: 10.1002/anie.201911477.

[28] Jiang R, Lu Y, Li L, et al. Mitochondria-targeted energy disruptor for augmented mild hyperthermia therapy of orthotopic lung cancer [J]. Adv Funct Mater, 2025, 35(49): 11217. doi: 10.1002/adfm.202511217.

[29] Weng J, Zheng G, Wen J, et al. Construction and application of microneedle-mediated photothermal therapy and immunotherapy combined anti-tumor drug delivery system[J]. Drug Deliv, 2023, 30(1): 2232950. doi: 10.1080/10717544.2023.2232950.

[30] Li Z, Cheng H, Wang B, et al. Polylysine-modified near-infrared-emitting carbon dots assemblies: amplification of tumor accumulation for enhanced tumor photothermal therapy[J]. J Colloid Interface Sci, 2024, 668: 132-141. doi: 10.1016/j.jcis.2024.04.153.

[31] 李劲松, 廖贵清, 李龙江, 等. 局部晚期口腔鳞状细胞癌PD-1抑制剂新辅助治疗专家共识(2026年版)[J]. 口腔疾病防治, 2026, 34(2): 105-118. doi: 10.12016/j.issn.2096-1456.202550582.
Li JS, Liao GQ, Li LJ, et al. Expert consensus on neoadjuvant PD-1 inhibitors for locally advanced oral squamous cell carcinoma (2026 edition)[J]. J Prev Treat Stomatol Dis, 2026, 34(2): 105-118. doi: 10.12016/j.issn.2096-1456.202550582.

[32] Li X, Xie X, Wu Y, et al. Microneedles: structure, classification, and application in oral cancer theranostics[J]. Drug Deliv Transl Res, 2023, 13(9): 2195-2212. doi: 10.1007/s13346-023-01311-0.

[33] Wang C, He G, Zhao H, et al. Enhancing deep-seated melanoma therapy through wearable self-powered microneedle patch[J]. Adv Mater, 2024, 36(11): e2311246. doi: 10.1002/adma.202311246.

[34] Liu D, Ali M, Benson HAE, et al. Local and systemic drug delivery using responsive microneedles[J]. ACS Nano, 2025, 19(49): 41459-41497. doi: 10.1021/acsnano.5c05949.

[35] Wu D, Zhao Z, Liu H, et al. *Escherichia coli* Nissle 1917-driven microrobots for effective tumor targeted drug delivery and tumor regression[J]. Acta Biomater, 2023, 169: 477-488. doi: 10.1016/j.actbio.2023.07.051.

[36] Wang Y, Liu S, Zeng Q, et al. Dual-functional nano-hydroxyapatite-based dressing combats melanoma recurrence and promotes wound healing after surgery[J]. Mater Des, 2026, 264: 115754. doi: 10.1016/j.matdes.2026.115754.

[37] Lei Q, He D, Ding L, et al. Microneedle patches integrated with biomineralized melanin nanoparticles for simultaneous skin tumor photothermal therapy and wound healing[J]. Adv Funct Mater, 2022, 32(22): 2113269. doi: 10.1002/adfm.202113269.

[38] Xiang Z, Wei X, Zhang Z, et al. Efficacy, safety and single-cell analysis of neoadjuvant immunochemotherapy in locally advanced oral squamous cell carcinoma: a phase II trial[J]. Nat Commun, 2025, 16(1): 3968. doi: 10.1038/s41467-025-59004-w.

[39] Wu Y, Chang X, Yang G, et al. A physiologically responsive nanocomposite hydrogel for treatment of head and neck squamous cell carcinoma *via* proteolysis-targeting chimeras enhanced immunotherapy[J]. Adv Mater, 2023, 35(12): e2210787. doi: 10.1002/adma.202210787.

[40] Miller S, Omoto N, DeCamp R, et al. Substantive dimethicone-based mucoadhesive coatings[J]. Materials, 2024, 17(22): 5590. doi: 10.3390/ma17225590.

[41] Liu J, Zheng W, Sun H, et al. Environment-adaptive microneedle design strategies for precision oral disease treatment: from material innovation to clinical translation[J]. J Control Release, 2025, 388 (Pt 2): 114402. doi: 10.1016/j.jconrel.2025.114402.

[42] Liu H, Sun Z, Yin M, et al. Polyphenol-modified Mg-Zn layered hydroxide-contained microneedle patch enhance mucosal repair by remolding diabetic oral microenvironment[J]. Adv Healthc Mater, 2025, 14(9): e2403883. doi: 10.1002/adhm.202403883.

（编辑　张琳）

Open Access
This article is licensed under a Creative Commons Attribution 4.0 International License.
Copyright © 2026 by Editorial Department of Journal of Prevention and Treatment for Stomatological Diseases

官网